IPTC-19914-Abstract

Combining Two- and Three-Phase Coreflooding Experiments for Reservoir Simulation Under WAG Practices

Leili Moghadasi, Eni SpA; Ehsan Ranaee, Deparment of Energy, Politecnico di Milano; Dario Renna, Martin Bartosek, Giuseppe Maddinelli, Franco Masserano, and Alberto Cominelli, Eni SpA; Fabio Inzoli, Deparment of Energy, Politecnico di Milano; Alberto Guadagnini, Deparment of Civil and Environmental Engineering, Politecnico di Milano

This paper was prepared for presentation at the International Petroleum Technology Conference held in Dhahran, Saudi Arabia, 13 – 15 January 2020.

Abstract

Enhanced oil recovery (EOR) processes may often involve simultaneous flow of two or three immiscible fluids inside the reservoir. A precise evaluation of relative permeabilities is critical to quantify multi-phase flow dynamics, assisting improved management and development of oil- and gas- bearing formations. This study illustrates the results of laboratory-scale investigations of multiphase flow on a sandstone reservoir core sample to evaluate relative permeabilities under two- and three-phase (i.e., water, oil, and gas) conditions. We use the ensuing information to simulate WAG injection at reservoir scale.

The experiments are conducted at high temperature, consistent with reservoir conditions, to obtain two- (oil/water and oil/gas) and three-phase (oil/water/gas) relative permeabilities through Steady-State (SS) technique. Our laboratory workflow allows for an improved investigation by combining coreflooding experiments with in-situ X-Ray evaluation of local saturation distribution. The latter technique permits to asses slice-averaged phase saturation along the rock core, enabling to compute saturation profiles and average saturations while flooding, thus yielding significant advantages over traditional methodologies based on mass balance.

Three-phase steady state (SS) experiments are performed by following diverse saturation paths, and the complete experimental dataset is provided to (*a*) assess the occurrence of local three-phase saturation conditions and (*b*) possibly investigate hysteretic effects of relative permeabilities. We evaluate three-phase relative permeabilities across the entire three-phase saturation region by leveraging a Sigmoid-based model (Ranaee et al., 2015).

The resulting set of experimental two- and three-phase coreflooding results constitute a unique dataset which is then employed for reservoir simulation studies mimicking WAG injection and results are discussed in comparison with reservoir production under a waterflooding scenario.

Key Words: Coreflooding, Relative Permeabilites, Reservoir Simulations, WAG Injection, Saturation Path

Introduction

Description of multi-phase flow is challenging due to complexity of the phenomena involved, including, e.g., fluid-fluid interaction, surface and iterfacial tension effects, capillary trapping and wettability, all of which are strongly influeced by pore size distributions. In this context, a reliable characterization of system attributes such as relative permeabilities enables us to asses reservoir performance, and to provide robust estimates of gain in production associated with enhanced oil recovery techniques. Estimation of relative permeabilities can be performed through carefully conducted experimental campaigns, which are then interpreted on the basis of (available or new) (pseudo)empirical correlations. Dynamic methods mainly comprise Steady-State (SS) and UnSteady-State (USS) techniques. The latter approach has been shown to provide somehow discrepancies in the results (Dehghanpour et al. 2011, 2010; Kikuchi et al. 2005).

In the SS technique relative permeabilities are obtained by co-injecting all phases (e.g., water, gas and oil) in the porous medium. Injection is performed at fixed flow rates until steady state conditions are met. These constraints contribute to render SS experiments more time-consuming and expensive than their USS counterparts. In turn, a simpler data-elaboration and a more precise control over the saturation path is achieved, which renders this technique appealing for three-phase relative permeability estimation.

Relying on SS experiments enables one to clearly identify dependences of relative permeability on fluid saturation (e.g., Oak et al. 1990, Alizadeh et al. 2014 and references therein) and to define relationships between saturation path and the associated relative permeability values (i.e., providing a quantification of hysteresis effects). Otherwise, USS experiments yield robust controls only on end-points of the saturation space, thus requiring reliance on an a priori selected model to estimate the complete relative permeability curves.

Since relative permeability values largely depend on the proportions between volume fractions of fluids in a test sample, the accurate quantification of local fluid saturations is critical. Energy absorption techniques, such as X-ray or gamma-ray, are employed to provide descriptions of fluid saturations within core plugs during flow tests (Maloney 2003, Dehghanpour et al. 2010, Alizadeh et al. 2014).

It should be noted that evaluation of three-phase relative permeabilities are becoming increasingly relevant due to the increased importance of gas and Water Alternating Gas (WAG) injection schemes in field applications of enhanced oil recovery (EOR). Markedly, only a limited amount of published three-phase relative permeability dataset is currently available (e.g., Oak 1990, Oak et al. 1990, Dehghanpour et al. 2010, Masihi et al. 2012, Alizadeh et al. 2014). Experimental data for two- and three-phase flow conditions can be interpreted through various relative permeability models (e.g, Corey et al. 1956, Stone 1970, Stone 1973, Baker 1998, Ebeltoft 2013, Ranaee et al. 2015 and references therein).

Here, we focus on the results of a suite of laboratory-scale investigations of multi-phase (water/oil/gas) relative permeabilities performed on an unconsolidated reservoir sample. Relative permeabilities are obtained at reservoir temperature employing the SS approach for two- and three-phase settings. In-situ local saturation distribution is determined by X-Ray absorption measurements, with a closed-loop system allowing for recycling liquid phases and improved chemical equilibrium. Having at our disposal direct measurements of (section-averaged) saturation distributions enables robust characterization of relative permeabilities. Three-phase saturations are measured by relying on a dual energy X-Ray methodology and various saturation paths are explored. The collected dataset is then used to simulate a WAG injection scheme in a synthetic reservoir simulation model inspired by real field scenarios where oil and gas companies assess implementation of the EOR process we consider.

Material and Methods

Experimental Setup and Conditions. Figure 1 depicts a sketch of the experimental setup, a detailed description of our experimental setup is being illustrated by Moghadasi et al. (2016, 2019). The experimental setup consists of a hassler type core holder placed vertically in a saturation monitoring apparatus. X-Ray attenuation is employed to measure in-situ fluid saturation. The fluids are separated and recirculated using a closed loop system. The Steady-State (SS) method is employed to obtain accurate estimates of relative permeability curves.

The sample is vertically placed in a hassler-type core holder under a given confining pressure. A phase-separator is employed to separate (by gravity) the three fluids (wate, oil, gas) employed in the experiments. To avoid drying of core sample and alteration of water and oil composition, gas flows thorough a humidification system before being injected in the core. The humidification system consists of a vessel half-filled with oil and water and is kept at a constant temperature of 40°C, where gas is bubbling from the bottom. Two pressure transducers are employed to monitor inlet and outlet pressure of the core, and (dry) gas flow rate was continuously monitored by a gas mass flow meter.

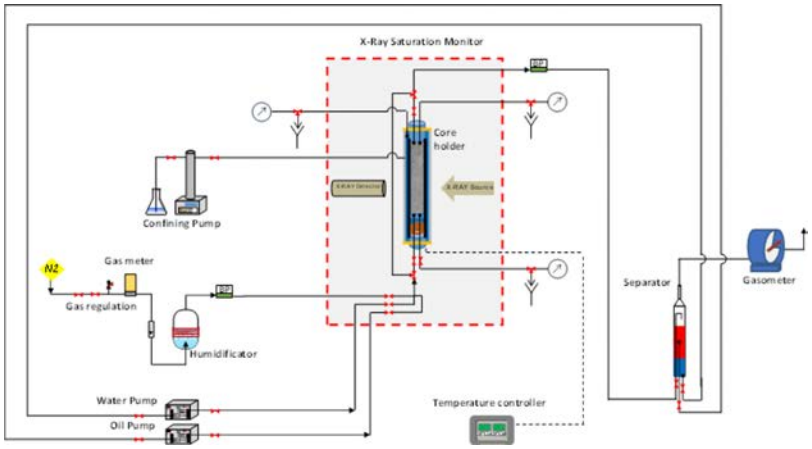

Figure 1—Sketch of the experimental setup (from Moghadasi et al 2019)

Experiments are conducted by considering various fluid flow rates and attaining saturation equilibrium for each of these. All experiments are conducted at a temperature of 68°C.

Core Sample and Fluids. The porous medium we considered is representative of an unconsolidated reservoir. It is 11.6 cm long and is placed inside a rubber sleeve (inner diameter of 5.08 cm) to pack the unconsolidated sandstone. A confining pressure of 90 bar is applied to stabilize the packing and prevent flow near the edges (Moghadasi et al 2019). The fluids used in the experiments are a mixture of (*i*) distilled water and (*ii*) different salts (e.g. NaCl and $CaCl_2$), sodium iodide (NaI) being used as X-Ray contrast agent, (*iii*) Nitrogen (N_2) gas, and (*iv*) decalin (decahydronaphthalene). Reservoir crude oil is employed during the ageing phase.

Two-Phase and Three-Phase Experimental Procedure. We perform various sets of experiments including two-phase water-oil, and oil-gas at residual water (S_{wr}), and three-phase (water-oil-gas) SS relative permeability experiments, characterized by different fractions of each phase in the injection streams, and sampling different saturation paths.

For two-phase experiments, water-oil imbibition (i.e. k_{rwo}, k_{row}) and oil-gas drainage (i.e. k_{rgo}, k_{rog}) relative permeability curves are assessed. In case of three-phase saturation, there is not a unique path from one point to another in the saturation space. In this case, saturation paths are constructed by imposing different

fractional flow of the phases and are denoted according to a standard three-letter system (Snell, 1862), corresponding to the variation of water, oil and gas, precisely in this order (C, D, and I stand for Constant, Decreasing, and Increasing, respectively).

The two-phase experiments start with the core being fully saturated with water. Then, to reach residual water (S_{wr}) condition, reservoir crude oil is injected at reservoir temperature and the sample is aged for a period of 4 weeks. Water-oil imbibition processes are applied sequentially through a series of SS injection steps to yield two-phase relative permeability curves (denoted as k_{rwo} and k_{row}, respectively). Drainage oil-gas relative permeabilities (denoted as k_{rgo} and k_{rog}, respectively) are assessed through joint injections of oil and gas by increasing gas and decreasing oil flow rates at S_{wr} conditions. Notably, crude oil is used only for aging, while flooding is based on decalin.

Three-phase SS experiments are performed by simultaneous injection of water, oil and gas into the sample for various initial saturation conditions, the latter imprinting the saturation path that the experiment follows. In case of CDI (Experiment denoted as EXP-1), the core is initially at saturation S_{wr}, and the fluid rates are changed until only gas flow is injected, to attain residual water and oil saturation.

The first DDI experiment (denoted as EXP-2) is performed on the core at residual water and gas saturation. Flow rates are set to yield high ratio of gas-to-water and gas-to-oil flow. Experiment IID (denoted as EXP-3) starts as the low gas-to-water and gas-to-oil flow ratio is achieved. At the end of IID, the second DDI experiment (denoted as EXP-4) is perfomed by maintaining a high ratio of gas-to-water and gas-to-oil flow.

Dual energy X-Ray attenuation is used to obtain multi-phase saturations. To achieve steady state conditions, approximately two days and four days are required for two- and three-phase experiments, respectively. X-Ray profiles provide section-averaged fluid saturations, with vertical resolution of 2 mm. Figure 2 depicts the schematic design of the experimental procedure employed for SS two- and three-phase core-flooding experiments.

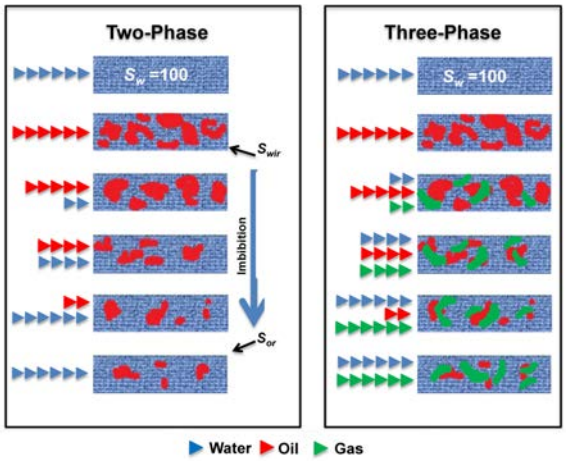

Figure 2—Schematic design of the experimental Steady-State (SS) two- and three-phase core-flooding procedure (Moghadasi et al. 2015, 2016)

Multi-Phase Relative Permeability and Saturation Estimates. In the context of the SS technique, pressure gradient and saturations are measured at steady-state conditions. Fluid properties, flow rates and pressure gradient are then employed to compute effective permeabilities through Darcy's equation.

A linear attenuation coefficient reflects the probability per unit length for an X-Ray to interact as it passes through a material and is a function of the atomic number and the bulk density of that material, besides the X-Ray energy (Maloney et al., 1999).

To avoid the complexity linked to the estimation of the attenuation coefficient for a complex rock matrix subject to an unknown X-Ray spectrum, a heuristic approach is here followed. The latter rests on a direct

correlation between X-Ray attenuation and saturations, which is characterized by acquiring X-Ray profiles of the sample at reference conditions.

In case of two-phase experiments, a single energy reading is adequate to calculate phase saturations, after readings of the sample at full saturation with each phase are available. Two-phase saturations are obtained by linear interpolation between the measured X-Ray attenuation and the values associated with the reference condition.

Multi-energy reading is required for three-phase experiments to correctly distinguish between the diverse phases. Three-phase saturations can then be computed by means of the following linear system:

$$\begin{cases} (C_w)_{E1} S_w + (C_o)_{E1} S_o + (C_g)_{E1} S_g = (C_{wog})_{E1} \\ (C_w)_{E2} S_w + (C_o)_{E2} S_o + (C_g)_{E2} S_g = (C_{wog})_{E2} \\ S_w + S_o + S_g = 1 \end{cases}$$

Here, $(C_w)_\alpha$, $(C_o)_\alpha$, and $(C_g)_\alpha$ are X-Ray readings corresponding to the setting where the sample is fully saturated by oil, water, and gas, respectively; $(C_{woh})_\alpha$ is the intensity for the three phase system; and a corresponds to the specific energy of the beam. The dual energies applied in this study are 55 kV-5 mA ($E1$) and 90 kV-4 mA ($E2$). A detailed description of the methodology employed is presented in Moghadasi al. (2016, 2019).

Results and Discussion

This section aims at providing an analysis of the impact of including information of coreflooding (both two- and three-phase) experiments in a field scale simulation of a WAG injection process. To this end, a synthetic reservoir model is built to represent typical geological conditions one may encounter in deep-water operations. The modeling process is described by first illustrating how the required three-phase relative permeabilities are derived from the available coreflooding data. Relevant information of the simulation model is provided, simulation results being finally illustrated and discussed.

Interpretation of two and three phase relative permeability data

Evaluation of the relative permeabilities for reservoir simulations relies on the availability of (*i*) two-phase water (k_{rwo}), oil (in the presence of water, k_{row}, and gas, k_{rog}) and gas (k_{rgo}) relative permeability; and (*ii*) three-phase water (k_{rw}), oil (k_{ro}), and gas (k_{rg}) relative permeability coreflooding dataset (see Figure 3).

We observed that water relative permeabilities display an approximately linear dependence on their own saturation when the latter is subject to a logarithmic transformation. Three-phase oil and gas relative permeabilities, when plotted against their own saturations, are more spreaded, when compared against the behavior of water relative permeabilities.

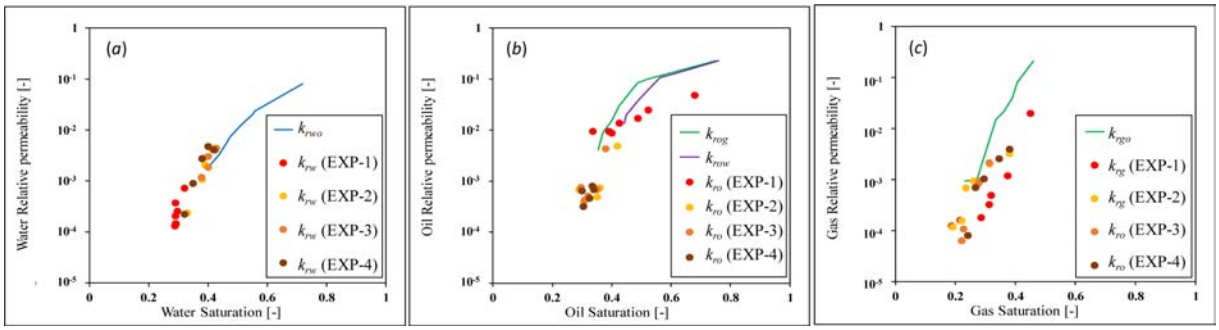

Figure 3—(a) water, (b) oil and (c) gas relative permeabilities collected through coreflooding experiments. Curves illustrate two-phase data, symbols representing data collected under three-phase experiments (i.e., EXP-1 to 4).

Relative permeability datasets (illustrated in Figure 3) comprise results from two-phase gas-oil drainage and water-oil imbibition conditions as well as three-phase waterflooding and gas injection experiments. Hence, with the available coreflooding dataset we solely consider hysteresis effects reflecting changes in the saturation paths from two- to three-phase conditions (and vice versa) and neglect cycle dependency of relative permeabilities due to possible switches of the saturation path between drainage and imbibition conditions. Thus, relative permeability of a given phase depends on saturation of all phases in our simulations. Figure 4a depicts the saturation values of the two- and three-phase experimental observations in a ternary plot. Figure 4a clearly shows that the collected dataset does not yield a complete coverage of the domain of three-phase saturations. We apply a three-phase relative permeability-hysteresis model, calibrated to the available dataset through a Sigmoid-based model (see Ranaee et al. 2015; 2017 for details on model and calibration workflow). The model is then employed for evaluating relative permeability across the saturation domain, as shown on Figure 4c, which accounts for two-phase relative permeability end-points, as well. Results of this analysis, expressed in terms of oil relative permeability values, are depicted in Figure 4d. Relative permeability values vary smoothly in the ternary saturation space (see Figure 4d) and can be used to evaluate k_ro for reservoir simulation under WAG injection. Numerical simulations are performed using a commercial toolbox (Schlumberger Geo-Quest 2010) which offers the capability of defining oil relative permeability as a function of both water and gas saturations through a two-entry table.

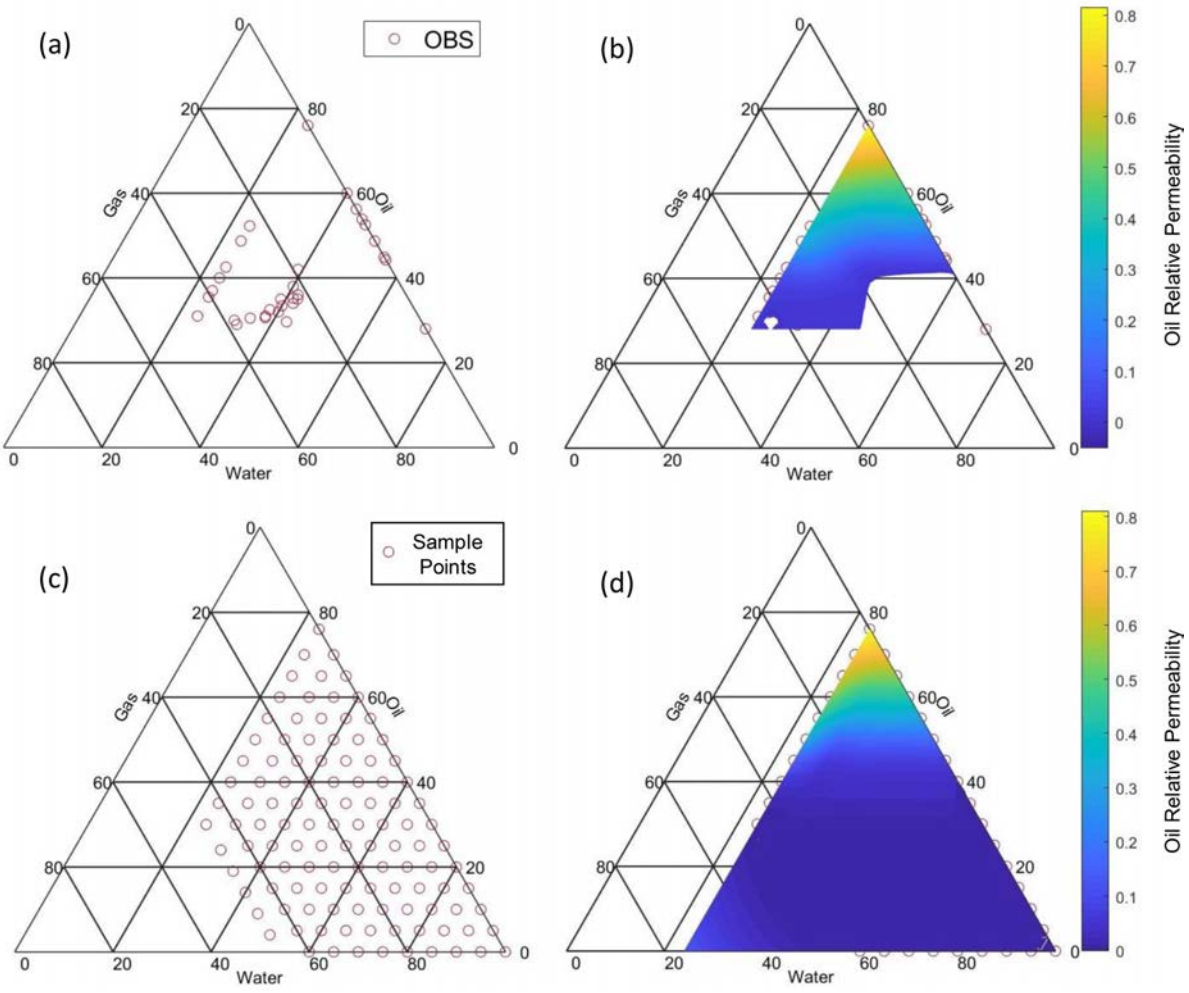

Figure 4—Ternary plot of (a) coreflooding observation ponts, and (b) related oil relative permeability values; (c) sample points employed to evaluate relative permeabilities by the Sigmoid-based relative permeability model, and (d) ensuing oil relative permeability values extrapolated to the whole saturation domain.

Reservoir model

The reservoir considered is discretized into 142×122×34 grid blocks. The setting is characterized by three injector (from I1 to I3) and five production (from P1 to P5) wells, as illustrated in Figure 5. Wells are completed differently across the 26 layers of the reservoir with a completion logic based on permeability patterns mimicking the results of deposition processes in a turbidite environment. The average reservoir thickness is about 550 ft (see Figure 5).

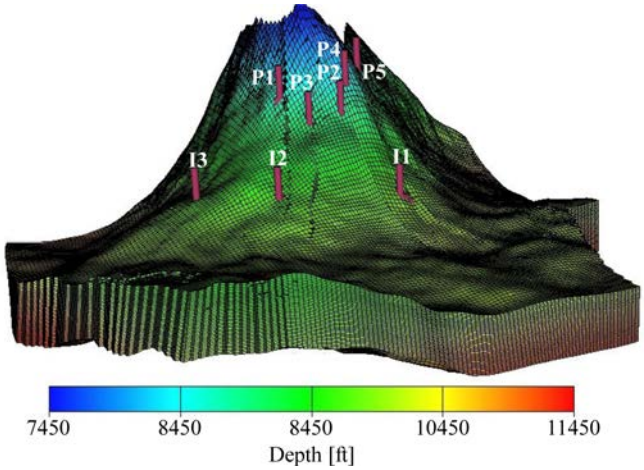

Figure 5—Geometry of the reservoir model considered, including depth of the computational cell centroids.

Maps of the spatial distribution of absolute horizontal (i.e., $k_x = k_y = k_h$) and vertical (i.e., k_z) permeability and porosity values are depicted inFigure 6a-c. Average porosity and horizontal permeability are 0.187 and 766 mD, respectively. Vertical permeability is set using three anisotropy ratios, $k_z / k_v = 0.01$, 0.1, and 0.4, reflecting increasing quality of the reservoir sand (see Figure 6b). Other relevant petrophysical attirubtes assigned to computational grid blocks, namely porosity and net-to-gross ratio, are shown in Figure 6c and in Figure 6d, respectively. The initial oil saturation distribution across the computational model is shown in Figure 6e. Notably, the reservoir is undersaturated with a buble point pressure much below the reservoir pressure and the water-oil contact (WOC) is included in the simulation grid which then comprises part of a surrounding aquifer. The initial pressure distribution (Figure 6f) is hydrostatic, with a reference pressure value $p = 4248$ psi at a reference depth of 9350 ft TVDssl.

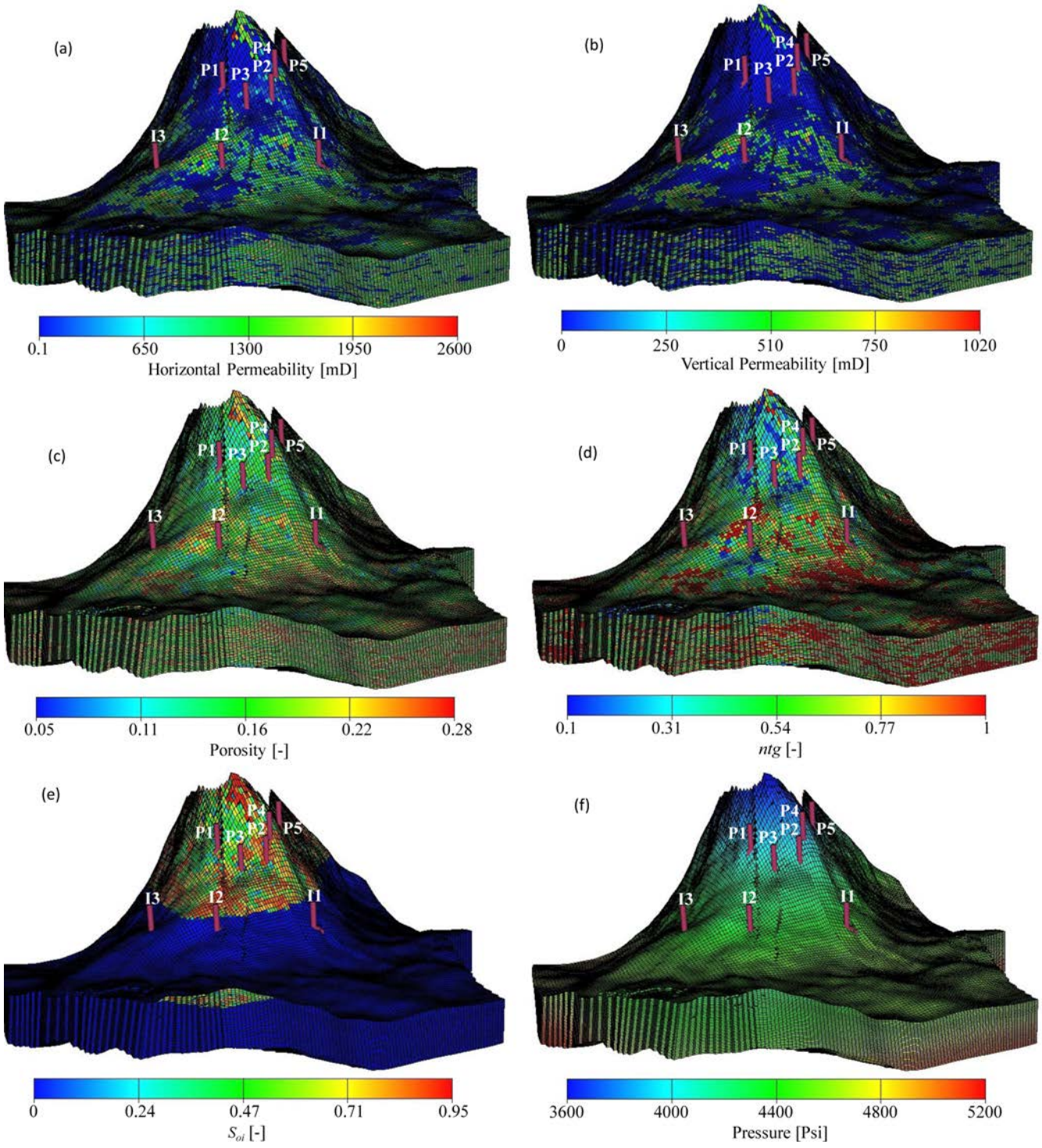

Figure 6—Spatial distribution of (a) horizontal permeability, (b) vertical permeability (c) porosity and (d) net-to-gross across the reservoir model; (e) oil saturation and (b) initial pressure state conditions at the onset of the simulations.

Density of water, oil and gas at standard conditions is set to 72.5×10^{-3}, 53.7×10^{-3} and 60.89×10^{-3} lb/ft^3, respectively. Figure 7 depicts Pressure-Volume-Temperature (PVT) properties of the reservoir live oil and dry gas, in terms of pressure evolution of the formation volume factor of water (B_w), oil (B_o), and gas (B_g).

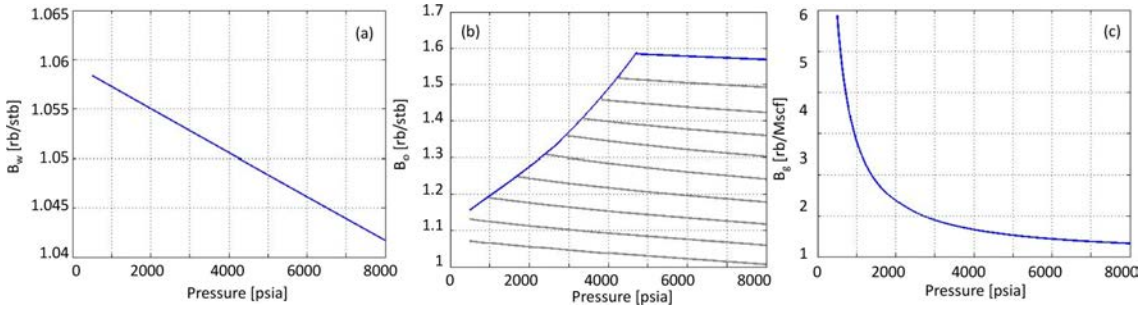

Figure 7—Dependence of the formation volume factor of (a) water (B_w), (b) oil (B_o), and (c) gas (B_g) on pressure. Each grey curve in Figure 5b corresponds to a given bubble point pressure, identified through the intersection with the solid blue curve.

Figure 8 depicts fluid viscosities versus pressure. One can note that viscosity of the water phase (μ_w = 0.42 cP) does not depend on pressure, viscosity of the oil phase (μ_w) showing a marked dependence on pressure and dissolved gas.

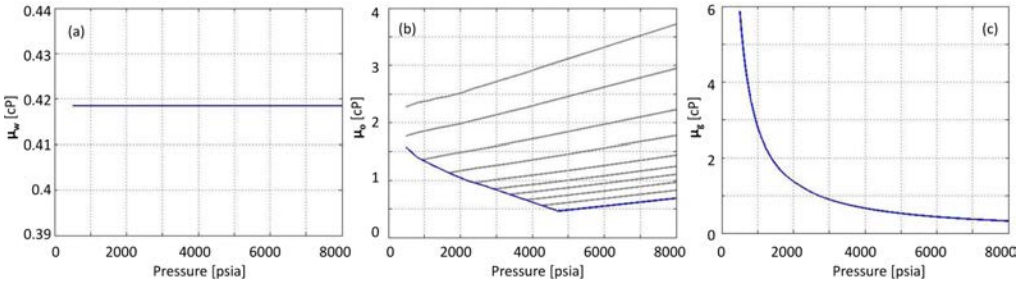

Figure 8—Dependence of (a) water (μ_w), (b) oil (μ_o), and (c) gas (μ_g) viscosity on pressure. Each grey curve in Figure 6b corresponds to a given bubble point pressure, identified through the intersection with the solid blue curve.

Relative permability for water, gas and oil are set as described in the previous section. It is assumed that the behavior of the reservoir rock resembles the one displayed by the porous media used in the laboratory experiments.

Simulation Results

Here, we present the impact of WAG injection on selected reservoir simulation outputs. We consider two simulation scenarios, corresponding to: (*a*) reservoir lifetime *waterflooding*, where all three injectors I1 (with 10000 stb/day), I2 (with 20000 stb/day), and I3 (with 10000 stb/day) inject water for a total production life, t_{LC} = 15 years; and (*b*) WAG injection (followed by 2 years of primary *waterflooding*), according to which after 2 years of primary water injection (with the same injector well control of the *waterflooding* scenario), we alternate gas injection and waterflooding at injectors I1 and I2 on an annual basis up to a total production life t_{LC} = 15 years. Injector I3 is set to *waterflooding* (with 10000 stb/day) during the whole WAG simulation time frame. Flow rates injected at I1 and I2 are set at 20000 stb/day during *waterflooding* and at 20000 Mscf/day during gas injection. Note that I2 is injecting gas when I1 is set for waterflooding and vice versa. Wells are technically constraint by bottom-hole pressure (BHP) limits, namely a value of 6000 psi as maximum for injection and a value of 1700 psi as minimum for production. P1 - P5 production wells operate at fixed liquid production rates of 15220, 4240, 5325, 5800 and 7700 stb/day, respectively.

Figure 9 depicts changes of the field pressure (FPR), water cut (FWCT), oil recovery fector (FOE) and gas-oil ratio (FGOR) versus simulation time. Figure 9a clearly shows that WAG injection can be useful to maintain reservoir pressure, when compared to the waterflooding scenario. As expected, both modeling strategies (i.e., waterflooding and WAG injection) provide a similar trend of oil recovery before water breakthrough (t < 7 years). A mild increase of FOE is noted for WAG injection afterwards, FWCT (mildly) decreasing and FGOR increasing following WAG implementation.

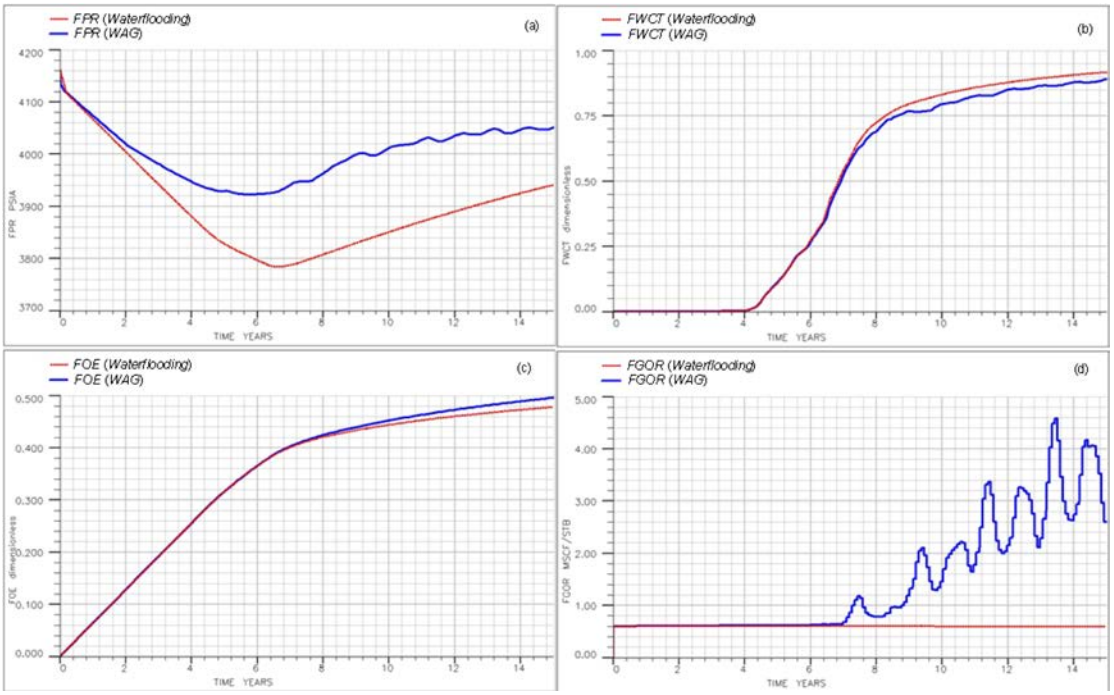

Figure 9—Temporal evolution of (a) FPR, (b) FWCT, (c) FOE and (d) FGOR across our simulation window for two different scenarios of waterflooding and WAG injection.

The mild effects observed for the WAG injection in improving ultimate oil recovery (4%) and decreasing watercut (3%), as compared to the waterflooding, can be related to the marked spatial heterogeneity (including the presence of faults) of the reservoir model characteristics. As such, some regions of the reservoir do not effectively contribute to the WAG effort. Figure 10 depicts results of water (WWPR), oil (WOPR), and gas (WGPR) production rates at production wells P4 and P1 under waterflooding and WAG injection practices. An increase of oil and gas production rates with a decrease of water production rate under WAG injection (compared to waterflooding case) in P4 is clearly evidenced in Figure 10b. Otherwise, production of oil in P1 appears not to be affected by WAG injection (as compared to the waterflooding scenario). These results clearly indicate that the success of a WAG injection practice to improve oil production may be markedly influenced by the complexity of the reservoir characteristics, the latter being a key element of investigation. As such, a reliable characterization of reservoir simulation model is a major block of a workflow leading to adequate estimate of reservoir performance, ultimate oil recovery, and study of the effectiveness of the different enhanced oil recovery scenarios.

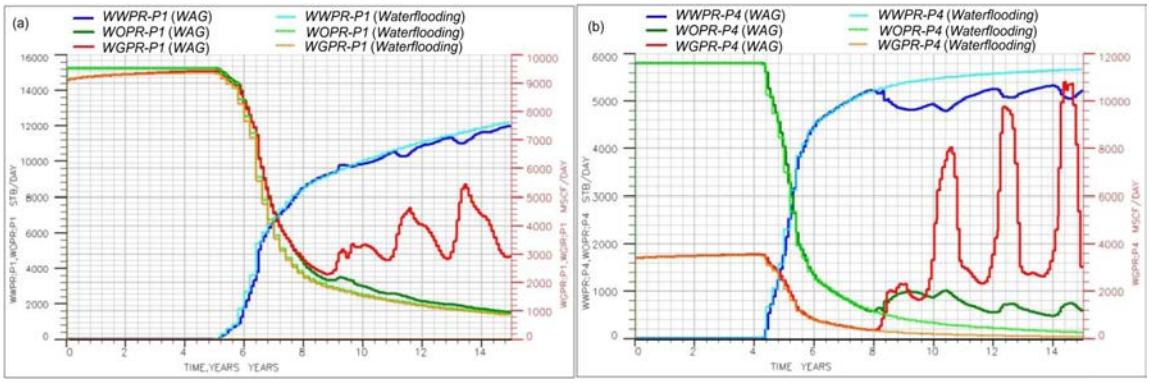

Figure 10—Water (WWPR), oil (WOPR), and gas (WGPR) production rates evaluated for (a) P1 and (b) P4 production wells under waterflooding and WAG injection scenarios.

Conclusions

Our work leads to the following key results:

1. The use of the in-situ X-Ray scanning technology enables us to accurately detect and quantify depth-averaged fluid displacement.
2. It was observed that in the studied case, water relative permeability does not exhibit hysteresis effects under two- and three-phase conditions and is a function of water saturation, consistent with the observation that water is the wetting phase in the experiments.
3. We provide a practical workflow to combine two- and three-phase relative permeability coreflooding datasets for reservoir simulation application under WAG injection practice.

Acknowledgements

The authors would like to thank Eni for granting permission to expose the results of these investigations.

References

Ahmadloo, F., K. Asghari and B. Y. Jamaloei. [2009] Experimental and Theoretical Studies of Three Phase Relative Permeability. In: SPE Annual Technical Conference and Exhibition, 4-7 October, New Orleans, Louisiana, 10.2118/124538-MS.

Alizadeh, A.H., Pin, M. [2014b] The effect of saturation history on three—phase relative permeability: an experimental study. In: *WRR*. **50** (2), 1636-1664. 10.1002/2013WR014914.

Baker, L.E. [1988] Three-Phase Relative Permeability Correlations. In: *SPE Enhanced Oil Recovery Symposium*, Tulsa, Oklahoma, http://dx.doi.org/10.2118/17369-MS.

Corey, A.T., Rathjens, C.H., Henderson, J.H. and Wyllie, M.R.J. [1956] Three-Phase Relative Permeability. In: *Journal of Petroleum Technology*, **8** (11): 63-65. http://dx.doi.org/10.2118/737-G.

Craig, F.F. [1993] The reservoir engineering aspects of waterflooding. In: Richardson, TX: Henry L. Doherty *Memorial Fund of AIME*, Society of Petroleum Engineers.

Dehghanpour, H., Aminzadeh, B., Mirzaei, M., DiCarlo, D. [2011] Flow Coupling During Three-Phase Gravity Drainage. In: *Phys. Rev. E*. **83**(6): 065302, 10.1103/PhysRevE.83.065302.

Dehghanpour, H., DiCarlo, D. A., Aminzadeh, B., Mirzaei Galeh-Kalaei, M. [2010] Two-Phase and Three-Phase Saturation Routes and Relative Permeability during Fast Drainage. In: *SPE Improved Oil Recovery Symposium*, Tulsa, Oklahoma, USA. http://dx.doi.org/10.2118/129962-MS.

Ebeltoft, F.L.E. [2013] Versatile Three-Phase Correlations for Relative Permeability and Capillary Pressure. In: *International Symposium of the Society of Core Analysis*, Napa Valley, California, USA. SCA **034** (2013): 1-14.

Hirasaki, G., Rohan, J. and Dudley, J. [1995] Interpretation of Oil/Water Relative Permeabilities from Centrifuge Displacement, In: *SPE Advanced Technology Series*, **3** (01): 66-75.

Kerig, P., Watson, A. [1986] Relative-Permeability Estimation from Displacement Experiments: an Error Analysis. In: *SPE Reservoir Engineering*, **1** (02): 175-182.

Kikuchi, M.M., Branco, C.C., Bonet, E.J., Zanoni, R.M. and Paiva, C.M. [2005] Water Oil Relative Permeability Comparative Study: Steady Versus UnSteady State. In: *International Symposium of the Society of Core Analysts*, Toronto, Canada. SCA **77** (2005): 1-7.

Liu. R., Liu. H., Li, X, Wang, J., Pang, C. [2010] Calculation of Oil and Water Relative Permeability for Extra Low Permeability Reservoir. In: International Oil and Gas Conference and Exhibition in China, 2010, 10.2118/131388-MS.

Masihi. M., Javanbakht, L., Horeh, F. B., Rasaei, M. [2011] Experimental Investigation and Evaluation of Three-Phase Relative Permeability Models. In: *Journal of Petroleum Science and Engineering*, 2011, **79** (1), 45-53, 10.1016/j.petrol.2011.08.017.

Maloney. D, Wegener, D., Zornes, D. [2000] Significance of Absorption Coefficients When Determining In Situ Core Saturations by Linear X-ray Scans. In: *SCA International Symposium of the Society of Core Analysts*, 2000, Abu Dhabi, UAE.

Maloney, D. [2003] X-Ray Imaging Technique Simplifies and Improves Reservoir-Condition Unsteady-State Relative Permeability Measurements. In: *Petrophysics* **44**(4): 271-278.

Maloney, D., Wegener, D., Zornes, D. [1999] New X-Ray Scanning System for Special Core Analyses in Support of Reservoir Characterization *SCA* **9940** (1999): 1-4.

Moghadasi, L., Guadagnini, A., Inzoli, F., Bartosek, M., Renna, D. [2016] Characterization of Two- and Three-Phase Relative Permeability of Water-Wet Porous Media through X-Ray Saturation Measurements. In: *Journal of Petroleum Science and Engineering*, 2016, **145**, 453-463. 10.1016/j.petro1.2016.05.031.

Moghadasi, L., Inzoli, F., Guadagnini, A., Renna, D., Bartosek, M., Maddinelli, G. [2017] Use of X-Ray Saturation Measurements in Flow through Investigations for the Characterization of Two- and Three-Phase Relative Permeability of Carbonate Rock In: Offshore Mediterranean Conference and Exhibition, Ravenna, Italy, OMC-2017-774.

Moghadasi, L., Guadagnini, A., Inzoli, F., Bartosek, M. [2015] Interpretation of Two-Phase Relative Permeability Curves through Multiple Formulations and Model Quality criteria. In: *Journal of Petroleum Science and Engineering*, 2015, **135**, 738-749. 10.1016/j.petro1.2015.10.027.

Moghadasi, L., Renna, D., Bartosek, M., Maddinelli, G., Scagliotti. S [2019] Experimental Investigation of Three-Phase Relative Permeability under Simultaneous Water and Gas (SWAG) Injection. >10R2019, *Pau. France*. 10.3997/2214-4609.201900078.

Naylor, P., Puckett, D. [1994] In-Situ Saturation Distributions: the Key to Understanding Core Analysis. *Society of Core Analysts Symposium*, Stavanger, SCA 9405.

Oak, M. J. [1988] A New X-Ray Absorption Method for Measurement of Three-Phase Relative Permeability. In: *SPE Reservoir Engineering*, **3** (01): 199-206. http://dx.doi.org/10.2118/14420-PA.

Oak. M. J. [1990] Three-Phase Relative Permeability of Water-Wet Berea. *In: SPE/DOE Enhanced Oil Recovery Symposium*, 1990, Tulsa, Oklahoma. 10.2118/20183-MS.

Ranaee, E., Inzoli, F., Riva. and Guadagnini, A. [2019] Hysteresis effects of three-phase relative permeabilities on black-oil reservoir simulation under WAG injection protocols, In: *Journal of Petroleum Science and Engineering*, **176**, 1161-1174, doi: 10.1016/j.petro1.2019.01.044.

Ranaee, E., Inzoli, F., Riva, M. Cominelli, A. and Guadagnini, A. [2018] Propagation to reservoir simulation of uncertainty associated with three-phase relative permeability models with hysteresis, SPE-190825-MS. Presented at SPE Europec featured at 80th EAGE Conference and Exhibition, 11-14 June, Copenhagen, Denmark doi: 10.2118/190825-MS

Ranaee, E., Moghadasi, L., Inzoli, F., Riva, M. and Guadagnini, A. [2017] Identifiability of parameters of three-phase oil relative permeability models under simultaneous water and gas (SWAG) injection. In: *Journal of Petroleum Scienceand Engineering*, **159**:942-951, 10.1016/j.petro1.2017.09.062.

Ranaee, E., Porta, G.M., Riva, M., Blunt, M.J., Guadagnini, A. [2015] Prediction of Threephase Oil Relative Permeability through A Sigmoid-Based Model. In: *Journal of Petroleum Science and Engineering*, **126**, 190-200, 10.1016/j.petro1.2014.11.034.

Schlumberger Geo-Quest. 2010. ECLIPSE 100 Reference Manual.

Stone, H.L. [1973] Stimation of Three-Phase Relative Permeability and Residual Oil Data. *J. Can. Petrol. Technol*. **12**, 53-61. http://dx.doi.org/10.2118/73-04-06.

Stone, H.L. [1970] Probability Model for Estimating Three-Phase Relative Permeability. In: *Journal of Petroleum Technology*, **22** (02): 214-218, http://dx.doi.org/10.2118/2116-PA.

Snell, R.W. [1962] Three-phase relative permeability in an unconsolidated sand J. Inst. *Petrol*., **48** (459) (1962), pp. 80-88